Structural phase transitions in $SbCl_5$-intercalated graphite

Hitoshi Homma* and Roy Clarke
Department of Physics, The University of Michigan, Ann Arbor, Michigan 48109
(Received 15 October 1984)

The structural behavior of $SbCl_5$-intercalated graphite has been investigated as a function of temperature and stage with use of x-ray diffuse scattering techniques. We present a global description of the ordering of the intercalant layers and their stacking arrangements, based on the existence of two segregated molecular species, $SbCl_3$ and $SbCl_6^-$. Strong interactions with the graphite host lead to a variety of long-period registered superlattices associated with the separate in-plane ordering of each molecular type. A new explanation for the structural phase transition at $T \approx 230$ K is presented in terms of a dipole-dipole coupling of $SbCl_3$ molecules.

I. INTRODUCTION

The unusual physical properties of metal-pentahalide graphite intercalates have been the subject of many studies over the past few years.[1,2] Much of this work was initially motivated by reports of highly anisotropic electronic transport, notably in AsF_5, where basal-plane conductivities approaching those of good metallic conductors are encountered.[3,4]

Recently a more general interest in this family of graphite intercalation compounds (GIC's) has developed as a consequence of their complex structural and chemical characteristics under various thermodynamic conditions. Surprisingly, however, very little is known as yet concerning the details of structural ordering in these molecular GIC's. Of particular importance in this respect is the configuration of intercalant molecules within the graphite host and its dependence on staging and temperature. In general, because of the molecular degrees of freedom, we expect even more intricate behavior than in the alkali-metal GIC's, which have shown such a rich variety of phase transition phenomena.[5]

The purpose of the present study is to examine in detail the molecular nature and phase transitions of one particular metal-pentahalide GIC, $SbCl_5$-intercalated graphite, using x-ray diffuse scattering techniques. We will see that the structural ordering is dominated by the tendency to register (i.e., lock-in) to the graphite in-plane periodicity, thus forming *long-period superlattice structures*. This trend seems to be strongly characteristic of intercalation compounds[6] and underscores the importance of intercalant-host interactions. In fact, these systems are proving to be an excellent testing ground for studying the effects of *competing periodicities*, commensurability, and related domain-wall phenomena.[7–9] These materials are also of interest for the tendency of the intercalant to disproportionate upon intercalation into two distinct molecular species. We will present evidence for a heterogeneous microstructure such that islands of the minority species are dispersed in a monolayer matrix of the majority species. A further aspect, also related to the high degree of structural degeneracy in this class of materials, will be emphasized; namely, the quasi-two-dimensionality for stages $n \gtrsim 2$.

The layout of the paper is as follows. In Sec. II we describe the most important experimental details of our studies and, in Sec. III we discuss the stacking sequences of carbon and intercalant layers. In the main part of the paper, Sec. IV, we present our findings on a variety of new structural phases of $SbCl_5$-intercalated graphite and their ordering transitions as a function of temperature. In Sec. IV we also relate the various ordering phenomena to the unusual molecular nature of the intercalated species.

II. EXPERIMENTAL PROCEDURE

A. Sample preparation

Single-crystal graphite flakes[10] (typical size $\sim 5 \times 5 \times 0.1$ mm^3) and highly-oriented pyrolytic graphite (HOPG) were used as host materials. Single-crystal samples are essential in experiments which probe the in-plane structure, whereas the polycrystalline HOPG samples are convenient for studies of the interlayer ordering. The sample of graphite to be intercalated was enclosed in a Pyrex ampoule with a small quantity (few cm^3) of liquid $SbCl_5$.[11] Normally, the graphite was not allowed to come into direct contact with the intercalant other than the vapor. In the two-zone method[12,13] employed here, the intercalant was heated to a temperature T_i and the graphite was maintained at some higher temperature, T_g; for $SbCl_5$ GIC's, T_g is held in the range 440—480 K and a value of T_i (or $\Delta T = T_g - T_i$) is selected depending on the stage[14] required (see Table I).

In our experiments we have found that for cooking times of typically two days, well-ordered single stages are nearly always obtained, at least for the lower stages $n \leq 6$. In the framework of recent theoretical studies[15] of staging equilibria this implies large intercalant island sizes and/or a considerable degree of charge exchange in this system. We did not encounter difficulties with $(00l)$ line broadening and wave-vector shifts associated with stage disorder that were recently reported by Rayment *et al.*[16]

We have found it desirable to peel off the surface layers

TABLE I. Typical conditions for the intercalation of $SbCl_5$ into single-crystal and HOPG samples by the two-zone vapor intercalation method.

	Single crystal		HOPG	
Stage	T_g (K)	ΔT (K)	T_g (K)	ΔT (K)
1	440	0	440	0
2	473	10–70	453	10–60
3	473	110–120	453	70–80
4	473	135–140	453	85–100
5	473	145–150	453	120–140
6	473	~155	453	~160
7	473	~160	473	~180
8	473	~170	473	~200

of the graphite (with scotch tape) prior to inserting the sample in the intercalation ampoule. The purity of the reagent was generally found not to be important and 99% pure $SbCl_5$ was used to prepare most of the samples. However, for making stage 1, reproducible results could only be obtained by using high-purity $SbCl_5$.[17] The isobaric dissociation curve published by Mélin and Hérold[12] was used as a rough guide for preparing samples of a specific stage, although we found that the actual stability ranges for a given stage depend on the quality of the graphite host.

B. X-ray techniques

The experiments were carried out on a Huber four-circle diffractometer fitted with an offset χ circle. The latter was designed to hold a Displex-type closed-cycle cryostat. Samples were mounted directly on the cold finger of the cryostat after removing them from the intercalation ampoule; they were very stable against decomposition in the cryostat vacuum or when exposed to air, as judged by the constancy of $00l$ and $hk0$ peak intensities over a period of several weeks. This finding is in contrast to a recent report of intercalant desorption in samples prepared by a low-temperature photoassisted method.[16] Over longer periods, we found that some desorption and, consequently, mixed staging occurs when the samples are stored in air at room temperature; however, our results generally support the conclusions of previous authors[12,18] that $SbCl_5$ GIC's are remarkably stable in air.

During the x-ray experiments, thermal stability of typically ± 0.1 K was maintained by means of a TRI T-2000 temperature controller. For experiments above room temperature, the samples were mounted in a vacuum furnace which had a temperature stability of ± 1 K. The x-ray source was a Rigaku RU-200 rotating-anode generator operated at 55 kV and 150 mA. X rays from the molybdenum anode were monochromatized by means of a slab of HOPG of mosaic spread $\sim 0.4°$, giving a longitudinal resolution of 0.05 Å^{-1} full width at half maximum (FWHM). The transverse resolution was somewhat more relaxed in order to obtain greater x-ray intensity.

In the experiments described in this paper we employed a combination of photographic and diffractometry techniques. Oscillation and precession x-ray cameras fitted with cooling attachments were used for general surveys of reciprocal space; then samples were transferred to the diffractometer in order to obtain more detailed information on specific features of the diffraction patterns.

III. INTERLAYER STRUCTURE

A. Stacking sequences

We have investigated the stacking sequences of carbon layers and intercalant layers in stage-1–5 $SbCl_5$ GIC's based on HOPG. The stacking of carbon layers in pristine graphite, $ABAB\cdots$, may change upon intercalation into A/A or A/B, where the solidus refers to an intercalant layer.[1] These stacking sequences determine not only the crystallographic properties along the c axis, but also influence the in-plane intercalant structure.[2] A knowledge of the stacking of the intercalant layers is thus important in determining the correlation between these layers and whether intercalant atoms or molecules behave three or two dimensionally. This is of relevance to the effects of spatial dimensionality on phase transition phenomena.

Figure 1 shows a series of $(10l)$ scans through graphite (10) peaks ($k=2.94$ Å^{-1}) for stages 1 to 5, respectively. These scans probe mainly correlations in the stacking of the carbon planes. We also made higher-order scans through the graphite (11) peaks for stages 1 and 2 and obtained results consistent with the $(10l)$ scans. The expected $10l$ peak positions given by $ABAB$ stacking were compared with the experimentally observed positions for stages 1–5, taking a sandwich distance $d_s=9.42$ Å. High-precision measurements of d_s reveal that it is actually weakly stage dependent, and this aspect will be discussed in Sec. III B. The agreement with $ABAB$ carbon stacking is excellent and the results rule out the possibility of more complex arrangements such as ABC stacking.

The stacking of the intercalant layers was examined by taking diffractometer c^* scans through the $\sqrt{7}(10)$ superlattice reflection ($k=1.11$ Å^{-1}) for stages 1 to 5. Figure 2 shows the results for stages 1 to 3. The results for stages 4 and 5 are essentially the same as for stage 3. The stage 1 sample shows quasi-three-dimensional peaks at $k_{c*}=0.34$, 0.67, and 1.01 Å^{-1}. These wave vectors suggest the graphite $ABAB$ stacking sequence with two *distinguishable* intercalant layers (denoted by α and β). Thus the stage 1 stacking sequence is $A\alpha B\beta A\alpha\cdots$, for which

$$k_{c*}=2\pi/(9.42\times 2)=0.334\ \text{Å}^{-1}\ .$$

Here, the α and β layers are taken to be chemically identical but differ by an in-plane shift of $\frac{1}{3}\mathbf{a}_0\sqrt{7}+\frac{2}{3}\mathbf{a}_0\sqrt{7}$, where $\mathbf{a}_0,\mathbf{b}_0$ are the in-plane translation vectors of graphite. A microscopic rationale for the $\alpha\beta$ stacking will be given later in Sec. IV B 1.

The coherence length of the stacking, estimated from the peak FWHM after subtracting background, is found to be ~90 Å, which corresponds to only ten intercalant layers. For stage 2, the intercalant layer interaction dramatically decreases compared with stage 1; however, there can still be seen weak three-dimensional (3D) correlations in the form of broad c^* peaks. The peak positions $k_{c*}=0.23$, 0.72, and 1.21 Å^{-1} suggest a stacking sequence $AB\alpha AB\beta AB\alpha AB\beta\cdots$, for which

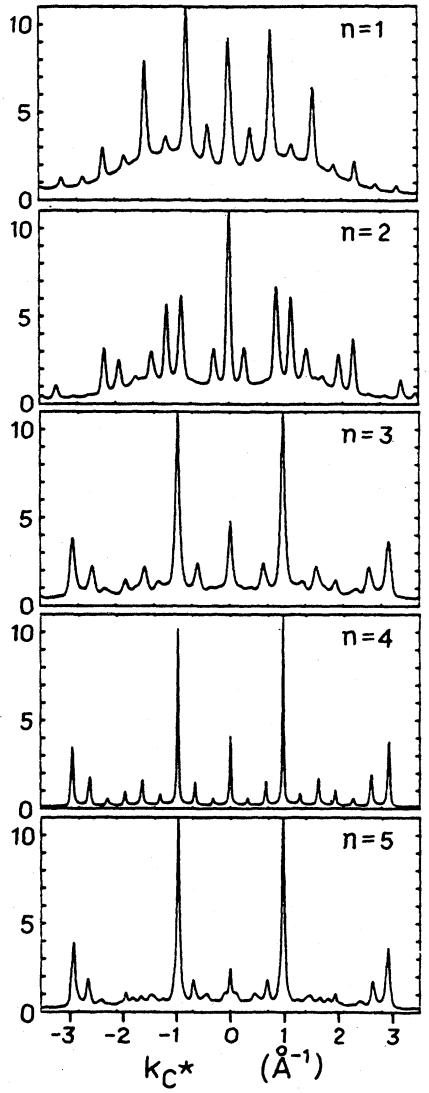

FIG. 1. (10l) scans through graphite (10) reflection for stages-1–5 $SbCl_5CiG$. The ordinate in each case is the x-ray intensity and k_{c*} is the wave-vector component normal to the layers. Note the diffuse contribution from the partially 3D correlated intercalant superlattice for stages 1 and 2.

$$k_{c*}=2\pi/(12.77\times 2)=0.246\ \text{Å}^{-1}\ .$$

The estimated c-axis correlation length for stage 2 is ~ 25 Å which corresponds to approximately two nearest-neighbor intercalant layers. For higher stages, $n \geq 3$, the stacking correlations of the intercalant are totally smeared out, i.e., a crossover to quasi-two-dimensional behavior occurs between stages 2 and 3.

We proceeded to calculate the structure factor $S(hkl)$ corresponding to the graphite c^* scans,

$$S(hkl)=\sum_j f_j \exp[-2\pi i(u_j h+v_j k+w_j l)]\ . \qquad (1)$$

where u, v, and w are the fractional coordinates of the basis and f_i are the atomic form factors. The model we adopted here was the simplest one, which is that the stacking of graphite layers maintains an ordered *ABAB* sequence, and we neglect the intercalant layers assuming they have random phases. In addition, we take into account the observation that all scans in Fig. 1 are *symmetric* with respect to the origin; this is due to stacking faults such that the graphite stacking is actually $ABAB\cdots AB//BABA\cdots BA//AB\cdots$, where the double solidus denotes a stacking fault. Thus, in the structure factor calculation, we took the average of these two configurations, i.e., $\frac{1}{2}[\,|S(hkl)|+|S(hk\bar{l})|\,]$. For stage 1, we could not obtain good agreement at all. The stage 2 case, however, showed a closer fit and for $n \geq 3$ the agreement with the experimental results was excellent, as shown in Fig. 3 for the $n=3$ case. Better results for stages 1 and 2 would be obtained by taking into account the in-plane superlattice structure and its $\alpha\beta$ stacking sequence which was not attempted here. To summarize, we established two aspects of the stacking:

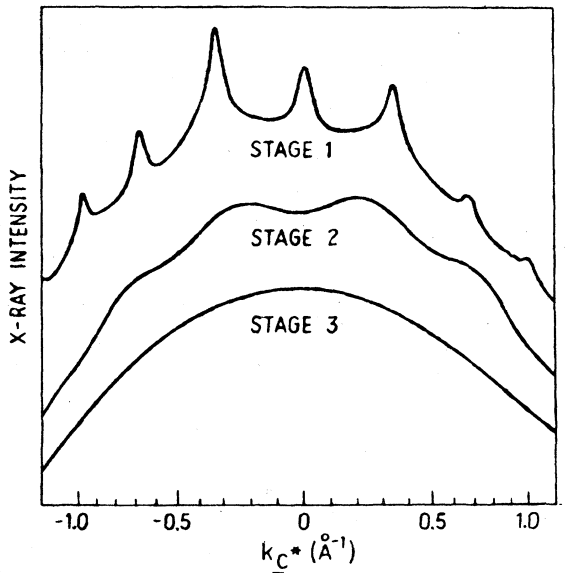

FIG. 2. c^* scan through a $\sqrt{7}(10)$ reflection showing a crossover from 3D to 2D correlations.

(a) The graphite stacking sequence in $SbCl_5$ GIC's for all stages is *ABAB*, which is the same as pristine graphite stacking, in agreement with previous studies.[19]

(b) Stage 1 shows partial 3D stacking coherence, and the higher stages, $n \geq 2$, show quasi-two-dimensional behavior.

The results suggest that in GIC's we may be able to study the crossover from 3D to two-dimensional (2D) behavior in a rather continuous way. Furthermore, we might also expect in-plane structural behavior in stage 1 which is different from that of the higher stages $n \geq 2$; this is indeed the case as we show below. The stage-2 sample is very interesting: being at the boundary of the 3D-2D crossover, weak modulation effects due to the interlayer interactions of intercalant are still noticeable. For stages $n \geq 3$, each

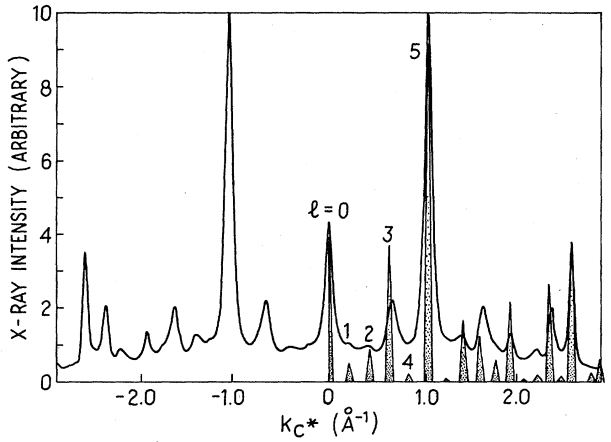

FIG. 3. Comparison of the calculated (shaded) and measured 10l graphite structure factor for stage-3 $SbCl_5$ GIC.

intercalant layer apparently behaves independently from other intercalant layers, somewhat analogously to adsorbed monolayers.

Note that the lack of intercalant stacking correlations for $n \geq 3$ persists down to low temperatures even into the "ordered" phase at $T \leq 230$ K (see Sec. IV). This is in contrast to the alkali-metal GIC's where in-plane ordering is ultimately accompanied by some degree of 3D interlayer ordering.[20,21] This difference in behavior probably reflects the greater susceptibility of the A/B sequence to stacking faults compared with the A/A stacking appropriate to alkali-metal GIC's.

B. Gallery spacing

A further manifestation of the dimensionality crossover described above is evident in the stage dependence of the carbon-intercalant-carbon sandwich distance, d_s. By applying Nelson and Riley's[22] extrapolation method to high-order 00l Bragg peaks we have been able to measure d_s with an order of magnitude better precision than previously reported values. Figure 4 shows the stage dependence of d_s for $SbCl_5$ GIC single crystals over the range $1 \leq n \leq 5$. Assuming a constant van der Waals carbon-carbon spacing of 3.35 Å, d_s is found to decrease between $n=1$ and 3 and then is stage independent for $n \geq 3$. This result is consistent with our observation of a crossover to quasi-two-dimensional behavior between $n=2$ and 3, but is different than the result of Mélin and Hérold[13] who found $d_s = 9.42$ Å for stage 1 and a roughly constant value of 9.36 Å for the higher stages. The stage dependence may also be related to variations in the degree of charge transfer. Note also that the gallery spacing is determined primarily by the majority molecular phase (see Sec. IV B). Small (static) variations in the gallery spacing due to the heterogeneous microstructure are evidenced by the larger than expected 00l Debye-Waller factor, being about an order of magnitude greater than the in-plane values for graphite.

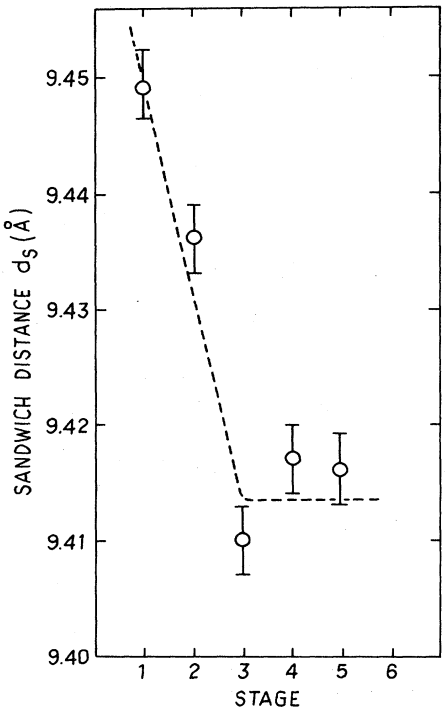

FIG. 4. Stage dependence of sandwich distance, d_s.

IV. IN-PLANE MOLECULAR ORDERING

A. Low-temperature structure

A typical in-plane diffraction pattern of single-crystal stage-2 $SbCl_5$ GIC at ambient temperature is shown in Fig. 5(a). It consists of a superposition of two types of x-ray scattering: commensurate $(\sqrt{7}\times\sqrt{7})R(\pm 19.11°)$ superlattice spots and a series of isotropic diffuse halos concentric with the origin, $k=0$. A similar pattern is observed for all $n \geq 2$. The first-stage in-plane structure is quite different in form and we defer discussion of this until later. On cooling the samples below $T \approx 230$ K, a large number of additional peaks appear in the pattern [Fig. 5(b)] growing continuously out of the diffuse scattering (see Fig. 6). This transition was first identified in electrical resistivity measurements by Fuzellier, Mélin, and Hérold.[23] The $\sqrt{7}\times\sqrt{7}$ peak positions remain accurately commensurate and resolution limited ($L \geq 500$ Å) through this transition and their intensities are essentially unaffected by the development of the new Bragg peaks. The latter tend to be somewhat broader than the $\sqrt{7}\times\sqrt{7}$ peaks and indicate in-plane coherence lengths of typically 100–200 Å.

The complex arrangement of spots that appear superimposed on the $\sqrt{7}\times\sqrt{7}$ diffraction pattern at $T \leq 230$ K is analyzed in terms of a superlattice of period $\sqrt{39}\times\sqrt{39}$.[24,25] For comparison, Fig. 5(c) is a calculated pattern based on a superposition of independent $(\sqrt{7}\times\sqrt{7})R(\pm 19.11°)$ and $(\sqrt{39}\times\sqrt{39})R(\pm 16.1°)$ hexagonal superlattices structures, taking into account the

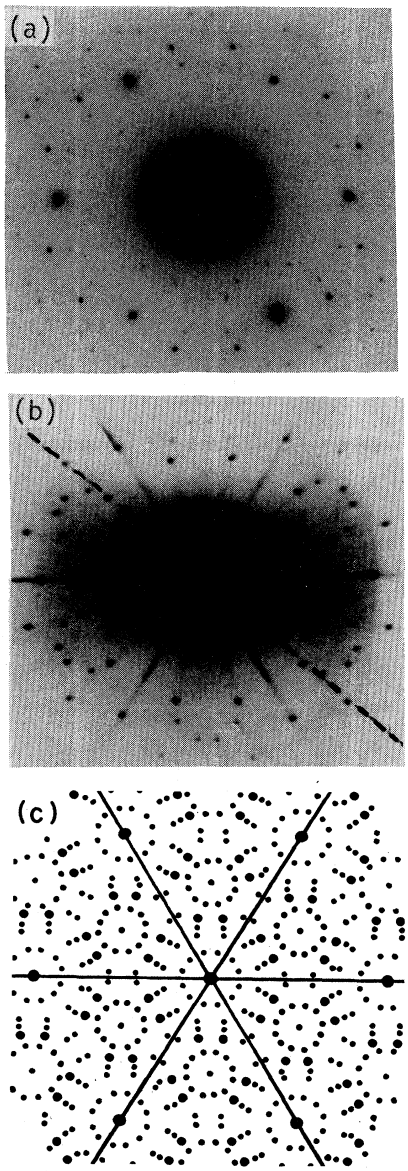

FIG. 5. In-plane diffraction patterns for stage-2 $SbCl_5$ GIC single crystals: (a) Ambient temperature, (b) $T=200$ K, (c) calculated pattern based on superposition of $\sqrt{7}\times\sqrt{7}$ and $\sqrt{39}\times\sqrt{39}$ superlattices.

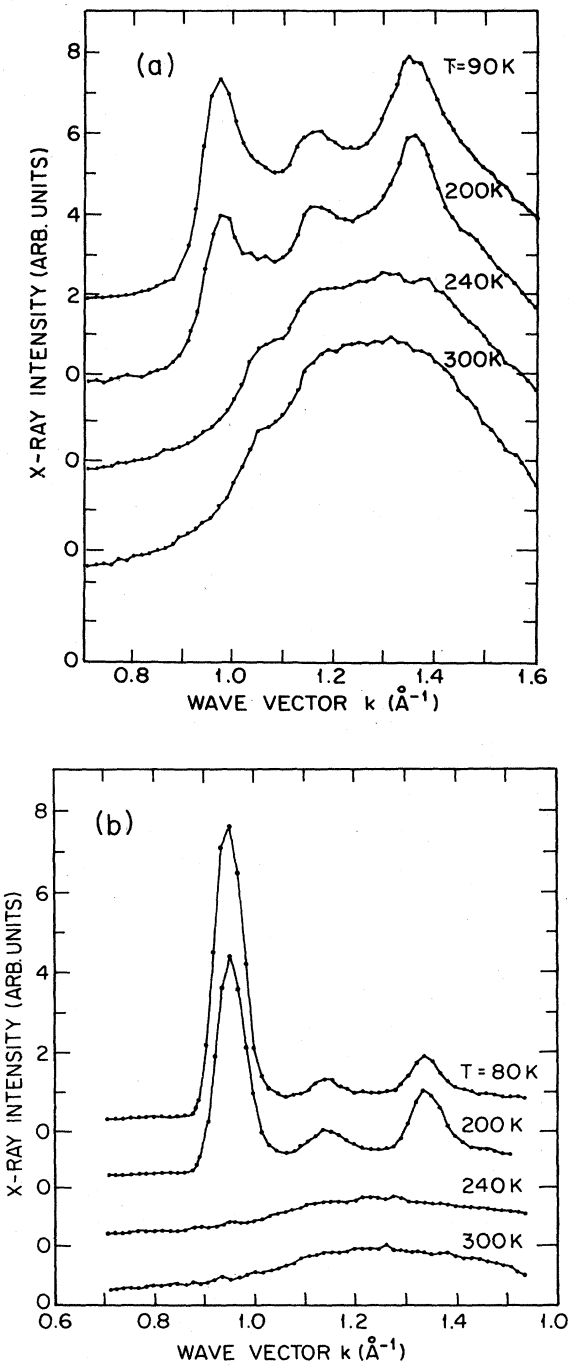

FIG. 6. Radial (θ—2θ) scan along dashed line in Fig. 5(b) at various temperatures. (a) Stage 2; (b) stage 3. Note the diffuse scattering at wave vector $k\approx 1.25$ Å^{-1}, as discussed in the text.

orientational twinning of these superlattices and the six-fold rotational symmetry of the graphite host.

Precise measurement of the wave vectors of the $\sqrt{39}$ peaks in the low-temperature diffraction pattern shows that they are not exactly commensurate with the $\sqrt{39}\times\sqrt{39}$ reciprocal lattice. The peaks are actually shifted slightly indicating that an in-plane structure is formed with a spacing approximately 2% compressed relative to the commensurate $\sqrt{39}$ periodicity. We have reported[24] previously that the wave-vector shifts do not correspond to a uniformly compressed lattice but rather to a *modulated* in-plane structure. The exact form of the modulations has not been investigated as yet; however, it is clear that some of the satellite reflections which are associated with higher-order graphite peaks are shifted to smaller wave vectors, the primary reflections being displaced towards larger wave vector relative to the commensurate $\sqrt{39}\times\sqrt{39}$ values.[24]

B. Molecular nature of the intercalant layers

The temperature independence of the $\sqrt{7}\times\sqrt{7}$ peaks, and the fact that the additional, low-temperature peaks are broader and originate from the diffuse scattering, suggest the presence of *two independent molecular phases* in this system: one being associated with a $\sqrt{7}\times\sqrt{7}$ superlattice and a second phase which undergoes a fluid-solid transition at $T_I \approx 230$ K. This temperature is found to be independent[24] of stage for $n \geq 2$, further evidence for the quasi-two-dimensionality of these samples.

The diffraction data presented above are entirely consistent with the suggestion made some years ago that certain metal pentahalides may undergo a disproportionation reaction upon intercalation into graphite:[26]

$$3MX_5 + 2e^- \rightarrow 2MX_6^- + MX_3 \ . \qquad (2)$$

Although considerable disagreement has risen regarding the applicability of this reaction to the intercalate for which it was originally suggested, AsF_5, there is mounting evidence that it provides useful insight into the chemistry of $SbCl_5$ GIC's. In particular, Mössbauer experiments[27] and an analysis of x-ray $00l$ structure factors[28] have both shown quantitative evidence for the existence of pentavalent ($SbCl_6^-$) and trivalent ($SbCl_3$) species in the ratio of approximately 1.9:1, close to the ideal value expected from completion of the reaction (2) above. Our x-ray results provide strong additional support for this picture; moreover, we will show that the detailed molecular nature of the interlayer structures and their phase transitions can be explained in terms of the products of such a disproportionation reaction.

1. $\sqrt{7}\times\sqrt{7}$ ordering

Consider, first, a close-packed layer of $SbCl_6^-$ molecules oriented with their trigonal axes normal to the carbon layers [see Fig. 7(a)]. The sum of appropriate ionic and van der Walls radii for this molecule[29] gives a gallery spacing d_s which is about 5% larger than that observed. This discrepancy indicates some degree of overlap, or registry, with the carbon layers such that the chlorine atoms are keyed to the honeycomb structure of the bounding layers. Indeed, the in-plane close packing, shown in Fig. 7(b), matches very well to a $\sqrt{7}\times\sqrt{7}$ superlattice of graphite. This arrangement gives a natural spacing between $SbCl_6^-$ molecules of $2\sqrt{3}r_{Cl} = 6.24$ Å, where r_{Cl} is the chlorine ionic radius, close to the observed commensurate spacing of 6.51 Å ($=\sqrt{7}a_0$). We will see later, in Sec. IV D 2, how this small misfit leads to a commensurate-incommensurate transition at $T \simeq 350$ K.

Not only does this packing explain the origin of the $\sqrt{7}\times\sqrt{7}$ superstructure, but it also provides a rationale for the *AB* stacking of the bounding carbon layers discussed in Sec. III A. In Fig. 7(b) it is clearly seen that the hcp conformation of the upper and lower chlorine layers, coupled with the graphite registry, dictates a *staggered* arrangement of carbon planes in this compound.

2. $\sqrt{39}\times\sqrt{39}$

One of the most intriguing questions in $SbCl_5$ GIC's is the origin of the peculiar long-period $\sqrt{39}\times\sqrt{39}$ superlattice. Noting that the $SbCl_3$ molecule has a rather large dipole moment[30] of 3.9 D (1.3×10^{-29} C m), we considered the possibility that a dipole-dipole pairing mechanism may be operative at low temperatures and could in fact be the driving force of the transition at $T \approx 230$ K. The molecular arrangement we propose, based on a pairing of $SbCl_3$ molecules, is shown in Fig. 8(a). The molecular

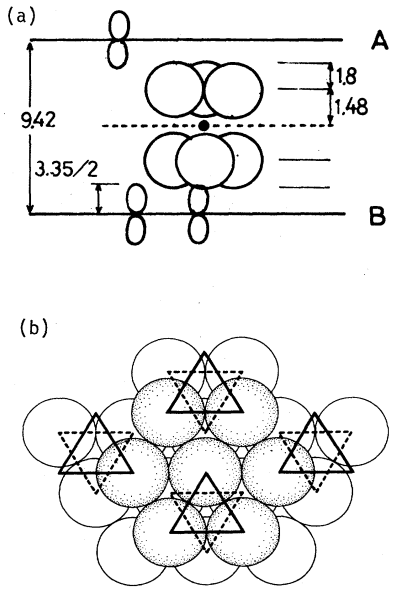

FIG. 7. (a) Orientation of $SbCl_6^-$ molecule. *A* and *B* denote staggered carbon planes. (b) Close packing of $SbCl_6^-$ molecules parallel to the graphite planes.

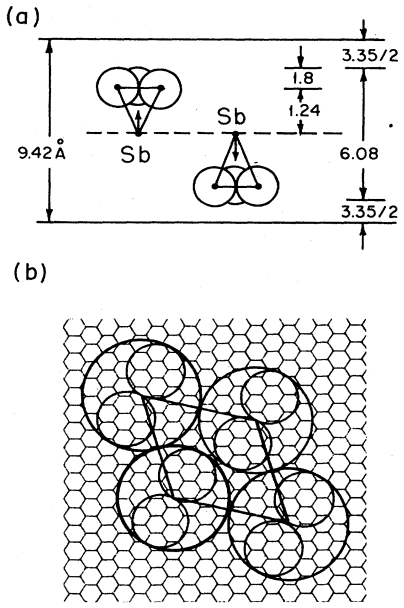

FIG. 8. (a) Pairing of $SbCl_3$ molecules. Note that the refined coordinates of Sb are displaced from the dashed line (see Fig. 9). (b) Packing of orientationally disordered $SbCl_3$ dimers (large circles) showing fit to $\sqrt{39}\times\sqrt{39}$ unit cell.

diameter corresponding to such a pairing is $(r_{SbCl_3}+r_{Cl})\times 4=15.2$ Å, where r_{SbCl_3} is the projection of the Sb—Cl bond[31] parallel to the carbon plane. This figure turns out to be very close to $\sqrt{39}a_0$ (15.36 Å), where a_0 is the in-plane graphite lattice spacing [see Fig. 8(b)]. Here we assume that there is negligable overlap of the in-plane projections of the $SbCl_3$ molecules. It is clear from Fig. 8(a) that there is space for a small overlap in the ordered phase; however, this would be forbidden at high temperature (where the average density of $SbCl_3$ molecules is determined) by the substantial orientational disorder. We also assume that at the temperatures of interest, $T\lesssim 230$ K, the $SbCl_3$-$SbCl_3$ pair is free to gyrate about an axis normal to the carbon layers. There is some recent calorimetric evidence[32] for a molecular ordering transition at somewhat lower temperatures ($T\approx 150$ K) which may be associated with the freezing out of this degree of freedom.

In our model for the $T=230$ K transition, therefore, we envisage a pairing of $SbCl_3$ molecules which, though orientationally disordered, are closely matched to a superlattice of the in-plane graphite structure; i.e., we suggest that the unusually large period ($\sqrt{39}a_0$) is a consequence of long-range dipolar forces within the $SbCl_3$ phase. It is instructive to calculate the interaction energy associated with the suggested dipole pairing. Taking a simple two-dimensional nearest-neighbor model with dielectric constant[33] $\epsilon=4$, we estimate the characteristic temperature of the dipole-dipole interaction to be 110 K. This is somewhat lower than the observed transition temperature, but the estimate is encouraging given the limitations of the calculation.

In the framework of our model, then, we interpret the diffuse scattering at $T\geq 230$ K (Fig. 6) as rising from positionally disordered $SbCl_3$ molecules. These would be expected to have much more mobility as single molecules than in the paired state. Even so, there seems to be insufficient space for a complete tumbling motion of these molecules in the high-temperature phase and in this context a "bridging" configuration has been suggested by Boca *et al.*[28] As mentioned above, the linewidths of the $\sqrt{39}$ peaks are well in excess of the resolution limit and we therefore suggest that islands of the $SbCl_3$ of about 100 Å in extent are dispersed within a relatively stable majority phase of $SbCl_6^-$ molecules. The islands can be solid or fluid depending on the temperature. Direct evidence for such a segregated microstructure was previously obtained from transmission electron micrographs[24] and, more recently, x-ray fluorescence from the different species has been reported.[34] In the following section we present a structure factor calculation based on our model which gives good qualitative agreement with the observed (00l) intensities.

C. Chemical aspects of intercalant layers

Using expression (1), corrected for Lorentz, polarization, and Debye-Waller factors, we attempted to fit (00l) peak intensities for the various stages. We assumed only two molecular species as described above, ignoring the possibility of other phases such as $SbCl_4^-$ raised by Boolchand *et al.*[27] In the least-squares-fitting procedure several adjustable parameters were introduced: (i) an overall scaling factor, (ii) the ratio n_0 of the intercalant concentration relative to the carbon atom concentration in a single graphite layer, (iii) f_6/f_3, the relative concentration ratio of $SbCl_6^-$ and $SbCl_3$ (here n_0 and f_6 are chosen as independent variables), and (iv) the coordinates of the constituents of the intercalant molecules relative to the carbon layers. It was assumed that the $SbCl_3$ molecules have mirror symmetry with respect to the $z=0.5$ plane, i.e., Sb^{3+} up or down is equally likely [Fig. 8(a)]. Also, we assumed that the antimony and chlorine atoms were fully ionized (Sb^{5+}, Sb^{3+}, and Cl^-), the carbon atoms being neutral.

The best fit parameters for stages 2, 4, and 5 single crystals are shown in Table II. In agreement with a similar calculation[28] for $SbCl_5$ GIC's (stages 1—3), we commonly found $f_6/f_3\approx 2$, as predicted by the intercalation reaction (2). However, in contrast to earlier reports, which did not address the issue, we observed a large variation in the results from sample to sample. Although the 2:1 ratio was encountered in the great majority of samples studied, other samples showed ratios f_6/f_3 ranging from 1 to as much as 5. This indicates that the reaction does not go to completion in all samples, perhaps because of impurities and defects in some of the host crystals. The 00l intensity fits were rather insensitive to variation of the

TABLE II. Summary of parameters obtained from fits to 00l x-ray intensities of single-crystal samples. Sb positions are measured from the center of the intercalant sandwich and the coordinates of Cl ions are referred to the respective Sb ions (see Fig. 9). U_{33} is the mean square vibration amplitude normal to the layers and the residual R is defined by

$$R^2=\frac{\sum_l (\,|F^{\rm expt}(00l)|-|F^{\rm calc}(00l)|\,)^2}{\sum_l |F^{\rm expt}(00l)|^2}.$$

Between 15 and 20 peaks were included in the fitting procedure.

Stage	$z(Sb^{3+})$ (Å)	$z(Sb^{5+})$ (Å)	$z(Cl^-/Sb^{3+})$ (Å)	$z(Cl^-/Sb^{5+})$ (Å)	n_0	f_6/f_3	U_{33} (Å^2)	R
2	1.15	0	1.24	1.48	13.8	2.0	0.025	0.003
4		0	1.23	1.48	15.6	2.1	0.0	0.012
5	0.91	0	1.32	1.50	20.0	2.3	0.035	0.012

c-axis coordinates of the molecules compared with n_0 and f_6/f_3 and so we could not obtain very precise molecular coordinates (Table II). We did, however, confirm the previous observation of a splitting in the Sb^{3+} position to either side of $z=0.5$; the value we obtain, approximately ± 1 Å, is considerably larger than that reported earlier by Boca *et al.*[28] (± 0.07 Å). We do not know the reason for this discrepancy at present. The configuration resulting from the fits to $00l$ intensities is shown in Fig. 9.

It is interesting to note in Table II that the composition corresponding to the stoichiometry $SbCl_5$ $C_{n_0\times n}$ seems to vary in a systematic way with stage. Our measurements are consistent with those reported previously by Boca *et al.*[28] ($n_0=13.2$ for $n=1$, 13.5 for $n=2$, and 15.7 for $n=3$) whereas Mélin and Hérold[12] earlier reported a stoichiometry $n_0=12$. Within the framework of our model we can interpret the observed stage variations of the concentration in terms of $SbCl_6^-$ molecules arranged in a $\sqrt{7}\times\sqrt{7}$ superlattice (which on their own would give $n_0=14$) together with islands of $SbCl_3$ molecules having a $\sqrt{39}\times\sqrt{39}$ unit cell. Two different bases, which correspond to net composition $n_0=13.7$ or 15.8 including the $SbCl_6^-$ contribution with the observed 2:1 ratio, are shown in Fig. 10. The two values of n_0 are consistent with our experimental values, 13.8 for stage 2 and 15.6 for stage 4, and the difference may be understood as a consequence of pairing enhanced by the interactions of neighboring intercalant layers in stage $n\leq 2$ compared with those in stage $n\geq 3$. We further discuss the tendency towards $SbCl_3$ pairing at lower stages in the following section. Larger values of n_0 (e.g., $n_0=20$ for stage 5) are presumably a result of vacancies in the intercalant layers which are expected in the more dilute, higher-stage compounds.

Before leaving this topic we mention a strong correlation we have observed between the intensity ratios of specific $00l$ peaks and the parameters n_0 and f_6/f_3: The ratio f_6/f_3 is found[35] to be proportional to the relative intensities of diffraction orders $l=m_1$, and $l=m_1+1$ where $m_1=3$, 4, 5, and 6 for stages 2, 3, 4, and 5, respectively. On the other hand, n_0 is sensitive to the ratio of the intensities of $l=m_2$ and $l=m_1+1$ where $m_2=8$, 10, 12, and 14; this empirical relationship can be used for a fast and convenient characterization of the sample.

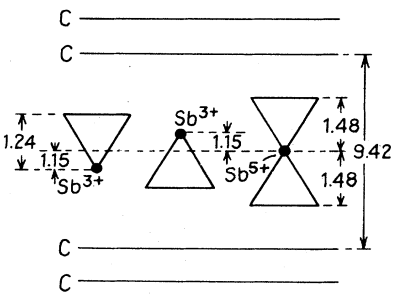

FIG. 9. Molecular configurations based on fits to the measured $00l$ intensities. Distances given in Å.

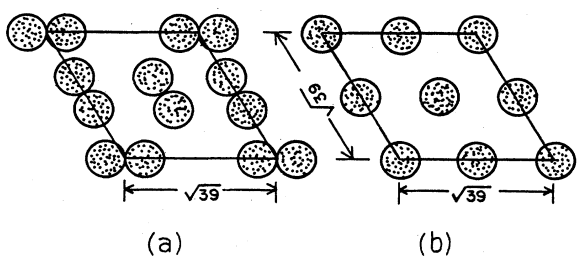

FIG. 10. Two possible unit cells for $SbCl_3$ molecules: (a) paired (appropriate to low stages), $n_0=13.7$; (b) unpaired (appropriate to $n\geq 3$), $n_0=15.8$.

D. Phase transitions

1. *Melting of* ($\sqrt{39}\times\sqrt{39}$) *phase*

We have identified the $T_I=230$ K transition in stage $n\geq 2$ $SbCl_5$ GIC's with the breaking of $SbCl_3$-$SbCl_3$ dipole pairs resulting in fluidlike $SbCl_3$ islands. The transition is strongly hysteretic, as seen in Fig. 11, and is apparently very sluggish.[36] For this reason the measurements of the $\sqrt{39}(20)$ superlattice peak shown in Fig. 11 were taken very slowly over a period of approximately 12 h. Note also in some stage-2 samples a small residual intensity is observed at the $\sqrt{39}\times\sqrt{39}$ reciprocal-lattice positions, at temperatures *above* the transition temperature, T_I. This is the reason why, in Fig. 11, the intensity on heating falls below that on cooling for $T>T_I$. Further indications of residual $\sqrt{39}\times\sqrt{39}$ superlattice ordering up to room temperature in stage-2 samples were observed by Bittner and Bretz[32] in their recent heat-capacity studies.

No evidence for the persistence of $\sqrt{39}\times\sqrt{39}$ superlattice ordering at $T>T_I$ is observed in samples of stage $n>2$. This again suggests that *interlayer* interactions may enhance the stability of the $SbCl_3$ pairing suggested above, as may be expected if dipolar forces are involved. A

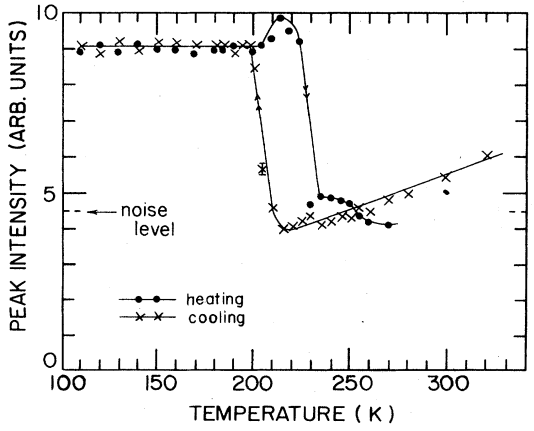

FIG. 11. Thermal hysteresis of $\sqrt{39}(20)$ peak in stage-2 $SbCl_5$ GIC.

direct confirmation that this is the case is seen dramatically in the behavior of the stage $n=1$ compound. In-plane diffraction photographs (Fig. 12) show that the $\sqrt{39}\times\sqrt{39}$ ordering is actually stable up to at least ambient temperature in stage-1 $SbCl_5$ GIC; moreover, rather than being incommensurate as in the case of $n\geq 2$ ($T<T_I$), the in-plane structure has locked in to an accurately commensurate $\sqrt{39}\times\sqrt{39}$ periodicity. These observations provide additional insight into the effects of three-dimensional interactions on the pairwise ordering of $SbCl_3$ molecules.

In view of the unusual microstructure of these GIC's it is important to note that the behavior of the $SbCl_3$ phase is likely to be dominated by finite size and boundary effects. The strongly hysteretic character of the transition, the broadening of the $\sqrt{39}\times\sqrt{39}$ peaks, and the time-dependent effects[36] at the transition, are all probably related to this unusual microstructure. We see no evidence for two transitions in this temperature range (180—230 K) as claimed by Rayment *et al.*,[16] and we suggest that the slow kinetics of stage ordering[37] and finite size of the islands may be responsible for the complex behavior of the c-axis lattice spacing that these authors reported. Nor do we observe the "glass transition" identified in recent electron-microscopy experiments by Timp *et al.*[25] It is possible that such a state may arise from the disruptive influence of a focused electron beam on the rather delicate molecular ordering arrangement described here.

2. $\sqrt{7}\times\sqrt{7}$ ordering

We now discuss the behavior of the $\sqrt{7}\times\sqrt{7}$ superlattice ordering as a function of temperature remembering that in the model presented here this phase arises from the close packing of $SbCl_6^-$ molecules. We have previously reported[38] that melting of this phase occurs at $T_m\approx 455$ K preceded by an incommensurate phase at approximately 350 K. Here, we provide additional information on this sequence of high-temperature transitions and relate the behavior to some recent theoretical predictions on substrate-mediated melting.

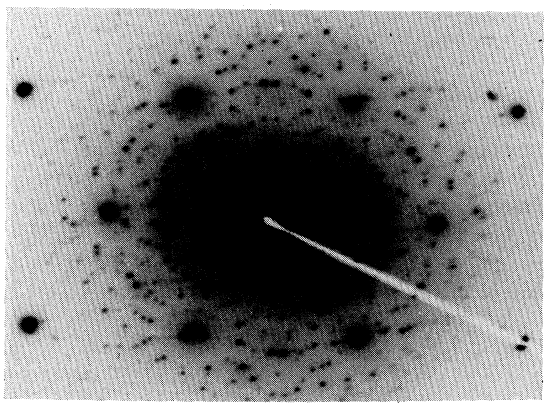

FIG. 12. In-plane diffraction photograph of stage-1 $SbCl_5$ GIC at ambient temperature [cf. Fig. 5(c)]. (Note: For clarity of reproduction we used electron diffraction to obtain this pattern; the results for x-ray diffraction are identical in this case.)

Figure 13 shows the temperature dependence of the $\sqrt{7}(10)$ peak position, and intensity, for stages 2 and 6. Both samples show a marked falloff in scattering intensity at this reciprocal-lattice position above room temperature. In addition, there is a sudden upwards shift in the wave vector of the $\sqrt{7}(10)$ peak at approximately 350 K, signaling a transition to an incommensurate phase which is 0.5—1.0% compressed relative to the commensurate $\sqrt{7}$ wave vector. A compression is expected based on the slightly smaller spacing in the close-packed arrangement (see Sec. IV B 1).

An important question raised by recent theoretical studies of the melting of commensurate overlayers on a substrate is the role of heterodomain fluctuations and associated topological defects such as domain walls.[39,40] Most

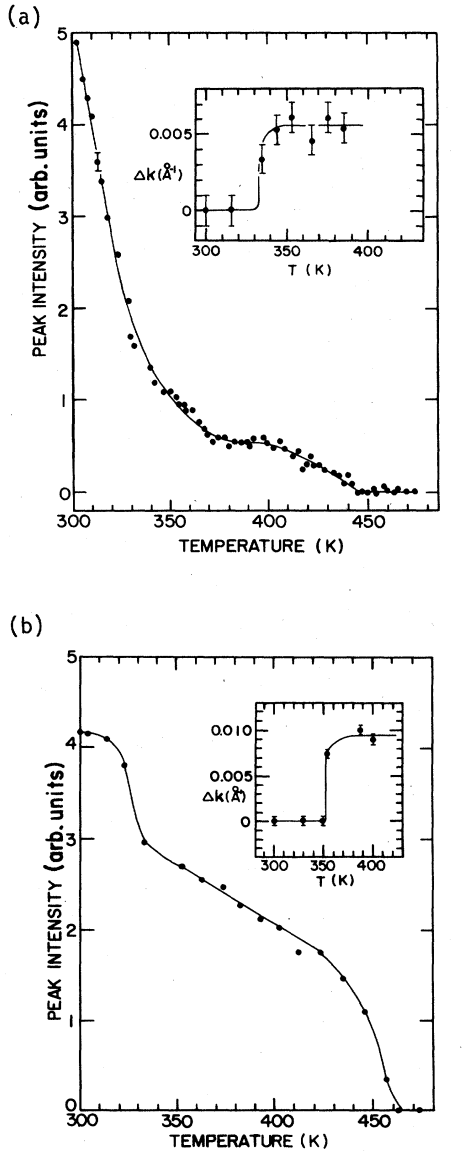

FIG. 13. X-ray peak intensity of $\sqrt{7}(10)$ reflection vs temperature. (a) Stage 6; (b) stage 2. The insets show the shifts of the peak wave vector as a function of temperature.

work to date has been concerned with overlayers of rectangular symmetry and detailed predictions are available for the uniaxial $p\times 1$ superlattice, where p is the ratio of the overlayer periodicity to the substrate lattice spacing. One of the most interesting findings is that a slightly incommensurate overlayer with degeneracy $p<\sqrt{8}$ is unstable to the formation of dislocations (domain walls); thus, sufficiently close to the commensurate-incommensurate (C-I) phase boundary, the overlayer should be fluidlike at all temperatures.[41] On the other hand, if $p>\sqrt{8}$ a solid-solid C-I transition is predicted at low temperatures. These predictions seem to be borne out experimentally in both the large-p and small-p regimes by observations on Br_2-intercalated graphite[8] ($\sqrt{3}\times 7$) and on Kr monolayers on graphite[42] ($\sqrt{3}\times\sqrt{3}$), respectively. The latter system has triangular symmetry and no rigorous determination of the critical degeneracy has been made for this case; however, the same general principles as in the uniaxial case should apply.

The triangular $\sqrt{7}\times\sqrt{7}$ superlattice, being close to the instability limit $p=\sqrt{8}$ (at least for rectangular geometry), is thus of some interest; particularly since the strong "substrate" effects characteristic of GIC's are expected to lead to well-defined domain walls. We have previously reported[38] that the steadily decreasing peak intensity with increasing temperature (Fig. 11) is not accompanied by a broadening of the radial peak width within the resolution of our scans. This implies that substantial in-plane coherence lengths are retained in the plateau region (350–450 K), perhaps favoring the solid-solid transition. However, a more revealing probe of the presence of domain-wall-type disorder is an azimuthal scan through the $\sqrt{7}(10)$ peak at constant wave-vector magnitude ($k\approx 1.11$ Å^{-1}). Figure 14 shows such a χ scan at two temperatures: in the commensurate phase ($T=300$ K) and at $T=380$ K, in the "incommensurate" phase. A series of χ scans shows that the scattering in the wings of the peak (in the χ direction) onsets abruptly at $T\approx 350$ K. This onset also coincides with the temperature at which the in-plane wave vector of the peak starts to shift. The wings become more and more pronounced as the temperature is increased to 450 K, above which the diffuse scattering is essentially isotropic. It is clear that there is a substantial amount of orientational disorder which gradually increases with temperature above $T\approx 350$ K, indicating the presence of misaligned, or meandering, domain walls. Thus the phase at $T\geq 350$ K is not a true solid with long-range bond orientational order even though the in-plane positional correlations are quite long ranged (> 100 Å). This behavior is consistent with the theoretical predictions for $p<\sqrt{8}$ discussed above. It is interesting to note that the transition to the isotropic fluid phase is spread over a large temperature range (> 100 K) as the domain wall disorder becomes progressively more severe, i.e., the instability with regard to dislocation formation is rather gradual in this case, possibly since $p=\sqrt{7}$ is close to the critical degeneracy. Note also that the in-plane mosaic of the intercalant layer at 8° FWHM is significantly worse than that of the graphite matrix (< 0.5° FWHM), even in the commensurate phase. This indicates that a significant density of domain walls are pinned[38] in this phase.

A further interesting feature of the χ scans shown in Fig. 14 is that the $\sqrt{7}$ peak rotates towards the (110) axis at the commensurate-fluid transition. This is a consequence of the twofold orientational degeneracy (see inset of Fig. 14) of the higher-order triangular superlattices such as $\sqrt{7}\times\sqrt{7}$, which produces two equivalent peaks at $\pm 10.89°$ relative to the (110) axis. Thus, as the heterodomain fluctuations become more prominent the distribution of orientations of registered domains is predominantly centered on (110). A similar effect has been reported in stage-2 CsC_{24} GIC (Ref. 20) and seems to be peculiar to asymmetric superlattices such as $\sqrt{7}\times\sqrt{7}$. The consequences of this orientational degeneracy have not been explicitly considered as yet in theories of substrate mediated melting, although the role of low-angle domain boundaries has been investigated in several recent studies.[43,44]

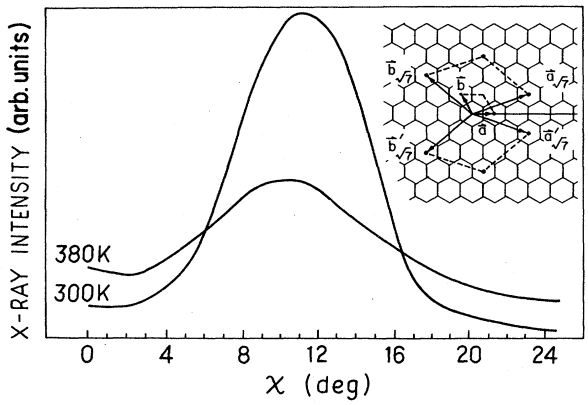

FIG. 14. Azimuthal scan through the $\sqrt{7}(10)$ superlattice peak at two temperatures. χ is the angle of the diffraction vector relative to the (110) reciprocal axis. Inset: Twin degeneracy of the $\sqrt{7}\times\sqrt{7}$ unit cell.

E. High-order commensurate superlattices

As a final topic in this paper we note that the orientational degeneracy discussed above can give rise to very-long-period in-plane superstructures which are multiples of the basic $\sqrt{7}\times\sqrt{7}$ unit cell. Figure 15 shows a diffraction pattern from such a sample and diffractometer scans confirm that this corresponds to a 14×14 superlattice which is commensurate to at least one part in 10^3. Note also the presence of diffuse rings in this pattern corresponding to those described in Sec. IV A which were related to a fluidlike $SbCl_3$ phase at ambient temperature. On cooling the samples below $T=230$ K, the diffuse rings again develop into the usual $\sqrt{39}\times\sqrt{39}$ pattern discussed above without any change in the 14×14 spots. This is further evidence that the $\sqrt{39}\times\sqrt{39}$ phase is segregated and is *not* a modulation of the $\sqrt{7}\times\sqrt{7}$ structure, in disagreement with the recent suggestion of Suzuki *et al.*[45]

The 14×14 superlattice can be understood in terms of a modulation of the $\sqrt{7}\times\sqrt{7}$ structure provided by the orientational twinning degeneracy shown in the inset of Fig. 14. The simplest modulation here is one in which the

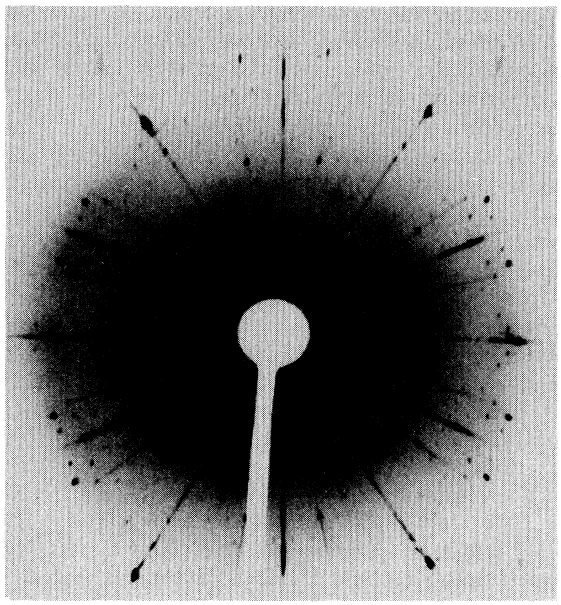

FIG. 15. In-plane diffraction pattern of a 14×14 superlattice in a stage-5 sample. The radial streaks are due to imperfect filtering of the x-ray beam.

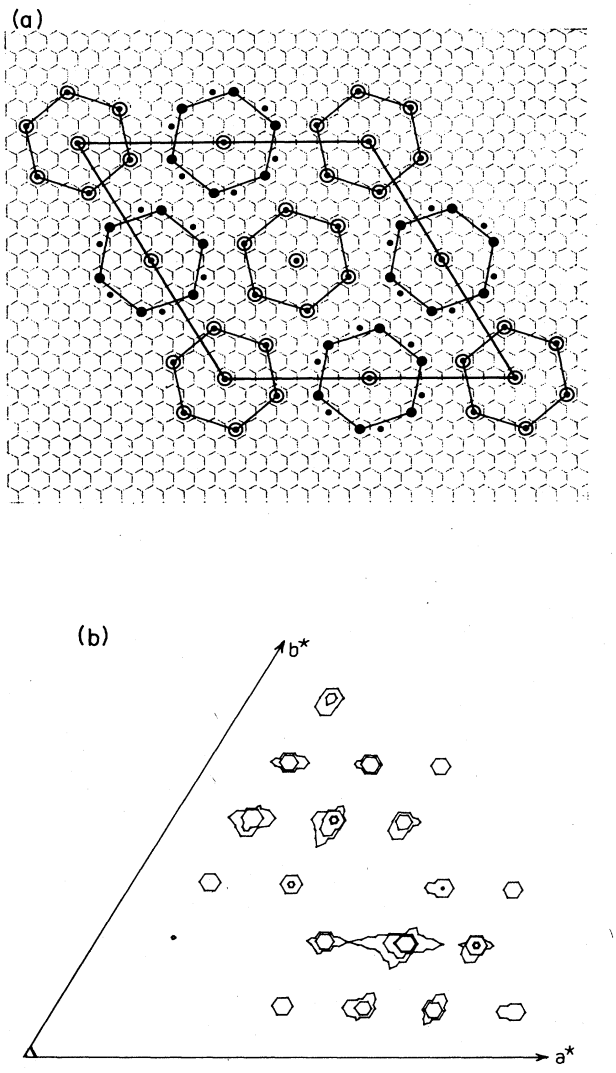

FIG. 16. (a) Model for (14×14) in-plane superlattice structure based on alternation of $\sqrt{7}$ translation vector orientation. The small circles and large circles indicate the two equivalent sets of sites for Sb corresponding to the two orientations of the $\sqrt{7}\times\sqrt{7}$ units (large hexagons). (b) Fourier transform of (a), omitting the contribution of Cl atoms.

orientation of the $\sqrt{7}$ translation vector alternates from one $\sqrt{7}\times\sqrt{7}$ unit to the next as shown in Fig. 16(a). The Fourier transform of this model is shown in Fig. 16(b); note that the model fits the relative intensities of the superlattice spots in Fig. 15 quite well; in particular note the unusual absence of reflections on the a^*_{14} and b^*_{14} axes.

A still higher-order commensurability is observed in some samples: 28×28 [see Fig. 17(a)], corresponding to an in-plane repeat of ~70 Å. In the translation vector alternation model introduced above, such an arrangement would be formed by two $\sqrt{7}\times\sqrt{7}$ units with one orientation followed by two units with the other orientation. This is schematically represented in Fig. 17(b) by taking an analogy with a modulated magnetic structure. Indeed, we speculate that the structures observed may be related to the ground states at the extremes of the anisotropic next-nearest-neighbor Ising (ANNNI) model phase diagram.[46,47] The $\sqrt{7}\times\sqrt{7}$ superlattice might therefore offer an interesting opportunity to study the complex manifold of modulated phases exhibited by this model. At temperatures somewhat above ambient, the higher-order superlattices are found to revert to an average $\sqrt{7}\times\sqrt{7}$ structure. For example, the 14×14 superstructure reflections disappear at $T\approx343$ K, a first-order phase transition.[35] The long-period ordering is completely reversible and represents a stable thermodynamic state of the in-plane structure. The discontinuous nature of the transition is consistent with the expected dominance of fluctuations in this quasi-two-dimensional system.[48]

We have not yet been able to identify the particular chemical composition, coverage, and preparation conditions that lead to this kind of ordering since the effect is seen in only a small fraction of the samples we have investigated, the normal $\sqrt{7}\times\sqrt{7}$ ordering being the general rule. We have observed long-period ordering in samples up to stage 6, but there does not seem to be any detectable difference in the composition of the intercalant layer (n_0 or f_6/f_3) compared with values for the more usual $\sqrt{7}\times\sqrt{7}$ samples. Thus changes in the chemical potential and free energies leading to the multiply modulated ordering must be rather subtle.

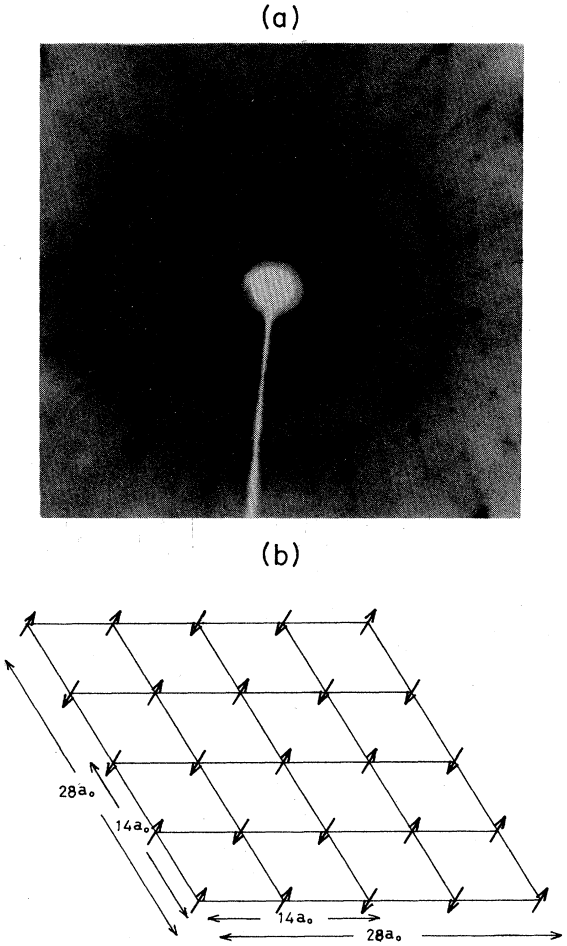

FIG. 17. (a) In-plane diffraction photograph of stage-3 single crystal showing (28×28) superlattice ordering. (b) Schematic representation of 28×28 superlattice.

V. CONCLUSIONS

We have presented a global description of the in-plane structure and stacking order of $SbCl_5$-intercalated graphite. We find compelling evidence for the presence of two segregated molecular species in the graphite host consistent with the disproportionation of the intercalant suggested by previous studies. Morever, the various structural phases and the transitions between them can be understood in terms of the products of such a reaction.

The in-plane ordering of the intercalant layers is dominated by strong interactions with the graphite host, resulting in a variety of long-period superlattice structures. In particular, the majority species $SbCl_6^-$ form a close-packed $\sqrt{7}\times\sqrt{7}$ arrangement and this also determines the stacking sequence of carbon and intercalant layers. A crossover to quasi-two-dimensional intercalant correlations is observed at stage $n>2$. Interspersed in the majority phase are islands of $SbCl_3$, some 100—200 Å in size. In stages $n\geq 2$ these are fluidlike at ambient temperature, and at $T\approx 230$ K the molecules order into an almost commensurate $\sqrt{39}\times\sqrt{39}$ superlattice. According to our model, this unusual structure originates from the pairing of $SbCl_3$ molecules coupled by long-range dipolar forces.

We have studied the order-disorder transition of the $\sqrt{7}\times\sqrt{7}$ phase in some detail and show that a highly correlated fluidlike phase precedes the transition to an isotropic liquid phase, in accord with recent theories of substrate-mediated melting of overlayers. Finally, we showed how the orientational twinning of an asymmetric superlattice ($\sqrt{7}\times\sqrt{7}$) can give rise to multiply modulated structures with high-order commensurabilities.

The details of the structural ordering presented here should help towards understanding the electronic, thermal, and transport properties of $SbCl_5$ GIC's and provide useful guidelines for similar studies in other complex molecular GIC's.

ACKNOWLEDGMENTS

It is a pleasure to thank M. J. Winokur and J. N. Gray for their help during the course of this work. We would also like to thank C. Uher, P. C. Eklund, P. M. Horn, and M. H. Jensen for stimulating discussions and M. Bretz for a careful reading of the manuscript. The research was supported by the National Science Foundation Low Temperature Physics Program Grant No. DMR-84-04975, and one of us (H.H.) received support from IBM Corporation.

*Present address: Argonne National Laboratories, Argonne, IL 60439.

[1]For an overview, see review by M. S. Dresselhaus and G. Dresselhaus, Adv. Phys. **30**, 139 (1981).
[2]R. Clarke and C. Uher, Adv. Phys. (to be published).
[3]F. L. Vogel, J. Mater. Sci. **12**, 982 (1977).
[4]S. C. Singhal and A. Kernich, Synth. Met. **3**, 247 (1981).
[5]S. A. Solin, Adv. Chem. Phys. **49**, 455 (1982).
[6]B. Schaub and D. Mukamel, J. Phys. C **16**, L225 (1983).
[7]R. Clarke, J. N. Gray, H. Homma, and M. J. Winokur, Phys. Rev. Lett. **47**, 1407 (1981).
[8]A. R. Kortan, A. Erbil, R. J. Birgeneau, and M. S. Dresselhaus, Phys. Rev. Lett. **49**, 1427 (1982).
[9]H. Homma and R. Clarke, Phys. Rev. Lett. **52**, 629 (1984).
[10]Natural graphite from a quarry near Harrisville (western Adirondacks region), New York.
[11]Supplied by Alpha Products, 99% purity.
[12]J. Mélin and A. Hérold, Carbon **13**, 357 (1975).
[13]J. Mélin and A. Hérold, C. R. Acad. Sci. Ser. C **269**, 877 (1969).
[14]A. "stage-n" structure is defined as a repeating sequence of n host layers (carbon) followed by an intercalant layer.
[15]G. Kirczenow, Phys. Rev. Lett. **52**, 437 (1984).
[16]T. Rayment, R. Schlogl, and J. M. Thomas, Phys. Rev. B **30**,

1034 (1984).
[17]Supplied by Johnson Matthey Co., 99.998% Puratronic grade.
[18]V. K. R. Murthy, D. S. Smith, and P. C. Eklund, Mater. Sci. Eng. **45**, 77 (1980).
[19]A. Hérold, in *Intercalated Materials,* edited by F. Lévy (Reidel, Dordrecht, 1979), p. 323.
[20]R. Clarke, N. Caswell, S. A. Solin, and P. M. Horn, Phys. Rev. Lett. **43**, 2018 (1979); M. J. Winokur and R. Clarke, *ibid.* **54**, 811 (1985).
[21]M. Mori, S. C. Moss, and Y. M. Jan, Phys. Rev. B **27**, 6385 (1983).
[22]J. B. Nelson and D. P. Riley, Proc. Phys. Soc. London **57**, 160 (1945).
[23]H. Fuzellier, J. Mélin, and A. Hérold, Carbon **15**, 45 (1977).
[24]R. Clarke, M. Elzinga, J. N. Gray, H. Homma, D. T. Morelli, M. J. Winokur, and C. Uher, Phys. Rev. B **26**, 5250 (1982).
[25]G. Timp, M. S. Dresselhaus, L. Salamanca-Riba, A. Erbil, L. W. Hobbs, G. Dresselhaus, P. C. Eklund, and Y. Iye, Phys. Rev. B **26**, 2323 (1982).
[26]N. Bartlett, B. McQuillan, and A. S. Robertson, Mater. Res. Bull. **13**, 1259 (1978).
[27]P. Boolchand, W. J. Bresser, D. McDaniel, K. Sisson, V. Yeh, and P. C. Eklund, Solid State Commun. **40**, 1049 (1981).
[28]M. H. Boca, M. L. Saylors, D. S. Smith, and P. C. Eklund, Synth. Met. **6**, 39 (1983).
[29]C. G. Vonk and E. H. Wiebenga, Acta. Crystallogr. **12**, 859 (1959).
[30]P. Kisliuk, J. Chem. Phys. **22**, 86 (1954).
[31]I. Lundqvist and A. Niggli, J. Inorg. Nucl. Chem. **2**, 345 (1956).
[32]D. N. Bittner and M. Bretz, Phys. Rev. B **31**, 1060 (1985).
[33]P. C. Eklund, D. S. Smith, and V. K. R. Murthy, Synth. Met. **3**, 111 (1981).
[34]D. M. Hwang, X. W. Qian, and S. A. Solin, Phys. Rev. Lett. **53**, 1473 (1984).
[35]H. Homma, Ph.D. thesis, University of Michigan, 1984.
[36]D. M. Hwang and G. Nicolaides, Solid State Commun. **49**, 483 (1984).
[37]S. A. Safran, Synth. Met. **2**, 1 (1980).
[38]H. Homma and R. Clarke, Phys. Rev. Lett. **52**, 629 (1984).
[39]P. Bak, Rep. Prog. Phys. **45**, 587 (1982).
[40]D. A. Huse and M. E. Fisher, Phys. Rev. Lett. **49**, 793 (1982).
[41]S. N. Coppersmith, D. S. Fisher, B. I. Halperin, P. A. Lee, and W. F. Brinkman, Phys. Rev. Lett. **46**, 549 (1981); Phys. Rev. B **25**, 349 (1982).
[42]D. E. Moncton, P. W. Stephens, R. J. Birgeneau, P. M. Horn, and G. S. Brown, Phys. Rev. Lett. **46**, 1533 (1981).
[43]D. Fisher, B. Halperin, and R. Morf, Phys. Rev. B **20**, 4692 (1979).
[44]D. J. Srolovitz, M. P. Anderson, G. S. Grest, and P. S. Sahni, Scr. Metall. **17**, 241 (1983).
[45]M. Suzuki, S. Tanuma, K. Suzuki, and M. Ichihara, Synth. Met. **6**, 121 (1983).
[46]M. E. Fisher and D. A. Huse, in *Melting, Localization, and Chaos,* edited by R. K. Kalia and P. Vashishta (Elsevier, New York, 1982), p. 259.
[47]P. M. Duxbury and W. Selke, J. Phys. A **16**, L741 (1983).
[48]B. Horovitz, T. Bohr, J. M. Kosterlitz, and H. J. Shulz, Phys. Rev. B **28**, 6596 (1983).

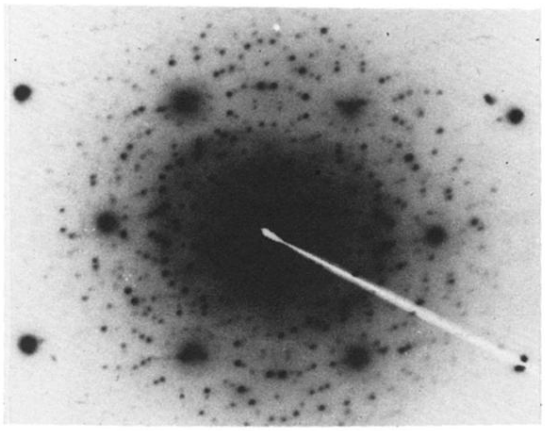

FIG. 12. In-plane diffraction photograph of stage-1 $SbCl_5$ GIC at ambient temperature [cf. Fig. 5(c)]. (Note: For clarity of reproduction we used electron diffraction to obtain this pattern; the results for x-ray diffraction are identical in this case.)

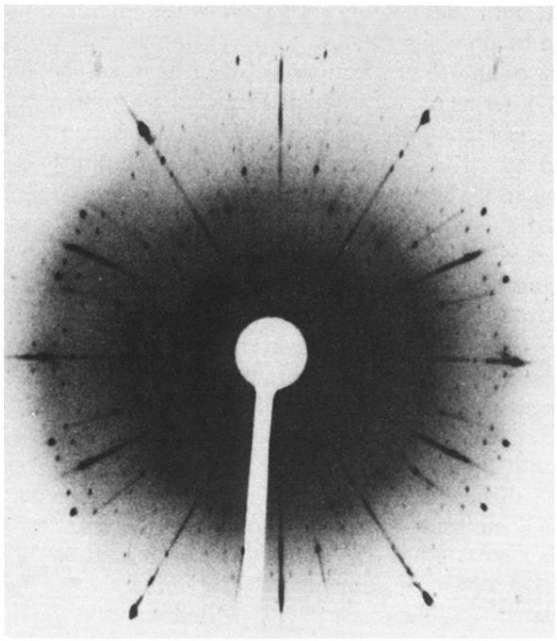

FIG. 15. In-plane diffraction pattern of a 14×14 superlattice in a stage-5 sample. The radial streaks are due to imperfect filtering of the x-ray beam.

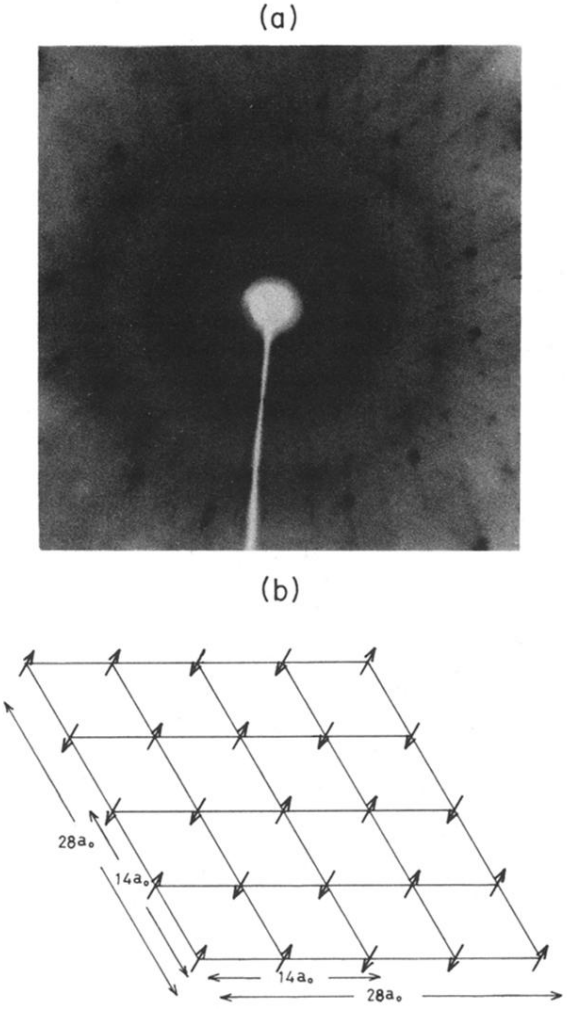

FIG. 17. (a) In-plane diffraction photograph of stage-3 single crystal showing (28×28) superlattice ordering. (b) Schematic representation of 28×28 superlattice.

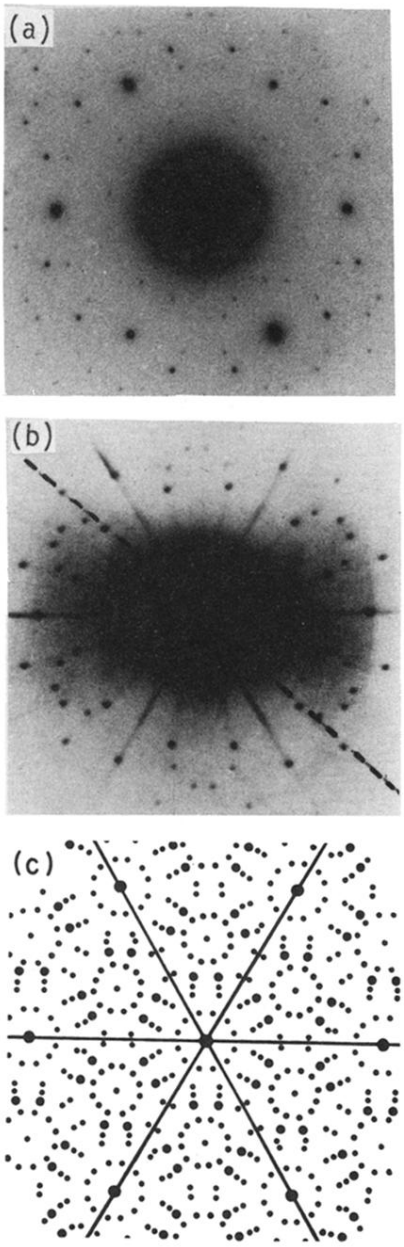

FIG. 5. In-plane diffraction patterns for stage-2 $SbCl_5$ GIC single crystals: (a) Ambient temperature, (b) $T=200$ K, (c) calculated pattern based on superposition of $\sqrt{7}\times\sqrt{7}$ and $\sqrt{39}\times\sqrt{39}$ superlattices.